CHEMISTRY
A EUROPEAN JOURNAL

DOI: 10.1002/chem.200700579

Selective Catalytic Oxidation of Ethanol to Acetic Acid on Dispersed Mo-V-Nb Mixed Oxides

Xuebing Li and Enrique Iglesia*[a]

Abstract: The direct oxidation of ethanol to acetic acid is catalyzed by multicomponent metal oxides (Mo-V-NbO_x) prepared by precipitation in the presence of colloidal TiO_2 ($Mo_{0.61}V_{0.31}Nb_{0.08}O_x/TiO_2$). Acetic acid synthesis rates and selectivities (~95% even at 100% ethanol conversion) were much higher than in previous reports. The presence of TiO_2 during synthesis led to more highly active surface areas without detectable changes in the reactivity or selectivity of exposed active oxide surfaces. Ethanol oxidation proceeds via acetaldehyde intermediates that are converted to acetic acid. Water increases acetic acid selectivity by inhibiting acetaldehyde synthesis more strongly than its oxidation to acetic acid, thus minimizing prevalent acetaldehyde concentrations and its intervening conversion to CO_x. Kinetic and isotopic effects indicate that C–H bond activation in chemisorbed ethoxide species limits acetaldehyde synthesis rates and overall rates of ethanol conversion to acetic acid. The VO_x component in Mo-V-Nb is responsible for the high reactivity of these materials. Mo and Nb oxide components increase the accessibility and reducibility of VO_x domains, while concurrently decreasing the number of unselective V-O-Ti linkages in VO_x domains dispersed on TiO_2.

Keywords: acetaldehyde · acetic acid · ethanol · molybdenum · oxidation · sustainable chemistry · vanadium

Introduction

The conversion of alcohols to aldehydes, ketones, and carboxylic acids by using stoichiometric oxidants (e.g., Cr^{VI}[1] and Mn^{VII} species[2]) leads to toxic waste by-products. Catalytic processes using O_2 or air as stoichiometric oxidants minimize the cost and environmental impact of these chemical processes.[3] Specifically, inorganic solids, easily separated from organic reactants and products, and gas-phase processes that avoid solid–liquid separations and use packed-bed reactors, would improve process efficiency. Inorganic catalysts for the oxidation of alcohols to aldehydes, ketones, and carboxylic acids typically consist of dispersed clusters of noble metals and their oxides (e.g., Pt,[4] Pd,[5] Ru[6]).

Ethanol has emerged as a fuel and a chemical feedstock available from biomass and could provide alternative routes to producing chemicals, such as acetaldehyde and acetic acid, currently produced from ethane, ethene, or methanol. Pd-based catalysts convert ethanol–O_2 reactants to acetic acid, but with low reaction rates and modest selectivities (433 K, 70–90% acetic acid selectivity; 0.2 g-acetic acid g-catalyst^{-1} h^{-1}).[7] Au clusters dispersed on $MgAl_2O_4$ convert aqueous ethanol solutions to acetic acid at ~453 K and 0.6 MPa O_2 pressure with yields of up to 90%.[8] Reducible oxides (e.g., Sn-MoO_x[9]) also catalyze this reaction (<60% acetic acid selectivity) at 423–573 K. A catalyst with VO_x as the active component (VO_x/TiO_2/clay) exhibited the best catalytic results for the oxidation of ethanol to acetic acid (97% acetic acid selectivity at 92% ethanol conversion).[10] A summary of previous reports is included in Table 1.

Multicomponent inorganic oxides containing V and Mo catalyze reactions of O_2 with alkanes to form alkenes and acids;[11] they also catalyze ethanol–O_2 reactions, but with low acetic acid productivities (0.02 g-acetic acid g-catalyst^{-1} h^{-1}) and modest selectivities (<70%).[12]

We have recently found that mixed Mo-V-Nb oxides precipitated in the presence of TiO_2 colloidal suspensions (P25, Degussa) give unprecedented acetic acid productivities and very high selectivities for the catalytic oxidation of ethane and ethene by using O_2.[13] These experiments showed that acetic acid synthesis rates are controlled by elementary

[a] Dr. X. Li, Prof. Dr. E. Iglesia
Department of Chemical Engineering
University of California at Berkeley
Berkeley, CA 94720 (USA)
Fax: (+1) 510-642-4778
E-mail: iglesia@berkeley.edu

Supporting information for this article is available on the WWW under http://www.chemistry.org or from the author.

Table 1. Summary of previous publications describing ethanol oxidation to acetic acid.

Catalyst	T[K]	Ethanol conv[%]	Selectivity[%] CH_3-CHO	CH_3-COOH	CH_3CO-OC_2H_5	CO_x	Synthesis rate [g g-catalyst^{-1} h^{-1}]
Pd-Te-Zn/SiO_2[a] Pd:0.86% Te/Pd=0.9 Zn/Pd=0.1 ref. [7]	433	90	1.4	92	3	3.1	0.244
Au/$MgAl_2O_4$[b] ref. [8]	453	97	–	85	–	15	0.90
Sn-Mo oxide[c] ref. [9]	548	100	20	60	1	19	0.55
VO_x/TiO_2/clay[d] ref. [10]	473	92	–	97	–	3	0.19
$Mo_{16}V_{5.6}Nb_{0.5}Sb_{0.3}Ca_{0.3}$[e] ref. [12]	528	98	0	66	0	20	0.022

[a] $C_2H_5OH:O_2:H_2O:N_2=2.5:6.25:25:66.5$; $P_{tot}=0.8$ MPa. [b] 150 mg catalyst, 1 wt% of metal, 10 mL of 5 wt% aqueous ethanol, 3 MPa total pressure, reaction for 4 h. [c] $C_2H_5OH:O_2:H_2O:N_2=3:24:13:73$; $P_{tot}=0.1$ MPa. [d] $C_2H_5OH:O_2:H_2O:N_2=2.5:3:5:89.5$; $P_{tot}=0.17$ MPa. [e] $C_2H_5OH:O_2:H_2O:N_2=2:6:6:86$; $P_{tot}=0.7$ MPa.

steps involving activation of C–H bonds in ethane, followed by hydrogen abstraction to form ethene and acetaldehyde; the acetaldehyde is then readily converted to acetic acid on Mo-V-Nb mixed oxides. The use of ethanol as a reactant, which we report here, circumvents these kinetic hurdles by providing reactants with more facile oxidative dehydrogenation routes to acetaldehyde than ethane or ethene reactants. The process and catalysts reported here exploit the remarkable reactivity of these dispersed oxides in the conversion of acetaldehyde to acetic acid by using O_2 and H_2O. The dispersed oxides described here as supported or unsupported oxides give 95% acetic acid selectivities and unprecedented catalyst productivities in a single-stage gas-phase ethanol oxidation process at modest reaction temperatures (~500 K).

Results and Discussion

Rates and selectivities were measured at 473–533 K by using C_2H_5OH (32 kPa) and O_2 (107 kPa). H_2O (0–640 kPa) was added because it increases acetic acid selectivity.[9] Helium (1130 kPa) was used to dilute reactants and avoid explosive mixtures. $Mo_{0.61}V_{0.31}Nb_{0.08}O_x/TiO_2$, prepared by precipitation of active components in the presence of colloidal suspensions of TiO_2 (24 wt% active components),[13] gave more than 90% acetic acid selectivities at complete ethanol conversion (Table 2). Acetic acid synthesis rates (>1.0 g g-catalyst^{-1} h^{-1}) were much higher than on unsupported $Mo_{0.61}V_{0.31}Nb_{0.08}O_x$ (0.13 g g-catalyst^{-1} h^{-1}), but the two synthesis protocols gave similar acetic acid selectivities (Table 2).

Dispersing $Mo_{0.61}V_{0.31}Nb_{0.08}O_x$ structures onto TiO_2 colloidal suspensions led to higher total surface areas (34 $m^2 g^{-1}$; from N_2 physisorption measurements at its normal boiling point) than for bulk $Mo_{0.61}V_{0.31}Nb_{0.08}O_x$ (7.8 $m^2 g^{-1}$) and apparently also to a larger number of accessible active sites. It is not possible to determine the fraction of accessible surfaces consisting of $Mo_{0.61}V_{0.31}Nb_{0.08}O_x$ and uncovered TiO_2 directly from the unselective physisorption of N_2. We have therefore used CO_2 chemisorption at 313 K to measure the fraction of the total surface area consisting of exposed TiO_2.[14] These data show that about 82% of the TiO_2 surface was covered by $Mo_{0.61}V_{0.31}Nb_{0.08}O_x$ during precipitation of these active structures. From these data, we estimate the surface area of active $Mo_{0.61}V_{0.31}Nb_{0.08}O_x$ components in this sample to be 28 $m^2 g^{-1}$, whereas the surface area of bulk $Mo_{0.61}V_{0.31}Nb_{0.08}O_x$ powders is 7.8 $m^2 g^{-1}$. Areal acetic acid synthesis rates (normalized by these active surface areas) then become 16×10^{-8} and 7.7×10^{-8} mol $m^{-2} s^{-1}$ on $Mo_{0.61}V_{0.31}Nb_{0.08}O_x/TiO_2$ and $Mo_{0.61}V_{0.31}Nb_{0.08}O_x$, respectively. These comparable areal rates, and the similar selectivities in these two samples, indicate that the higher reaction rates (per mass of active component) measured on TiO_2-containing catalysts reflect a higher dispersion of active structures when such structures are precipitated in the presence of colloidal TiO_2. The slightly higher areal rate measured on the supported sample reflects a slightly higher catalyst temperature, caused by higher local bed temperatures on such highly active catalysts. The temperature of the $Mo_{0.61}V_{0.31}Nb_{0.08}O_x/TiO_2$ bed was about 10 K higher than for the unsupported $Mo_{0.61}V_{0.31}Nb_{0.08}O_x$ sample for the same heater temperature.

Primary acetaldehyde products were detected at low ethanol conversions, but their concentration decreased with increasing residence time (Figure 1), because of the role of acetaldehyde as an intermediate in acetic acid synthesis (Scheme 1), evidenced by the high acetic acid selectivity (95% at 100% acetaldehyde conversion) in the oxidation of acetaldehyde at 473 K. Esterification of acetic acid with ethanol led to small amounts of ethyl acetate; these equilibrium-limited reactions are favored at intermediate conversions, but are reversed as conversion increases, because ethyl

Table 2. Oxidation of ethanol to acetic acid on multicomponent metal oxide.[a]

Catalyst	T[K]	Ethanol conv[%]	Selectivity[%] CH_3-CHO	CH_3-COOH	CH_3CO-OC_2H_5	CO_x	Synthesis rate [g g-catalyst^{-1} h^{-1}]
24% $Mo_{0.61}V_{0.31}Nb_{0.08}O_x/TiO_2$	481	78	1.7	85	11	2.6	1.04
24% $Mo_{0.61}V_{0.31}Nb_{0.08}O_x/TiO_2$	510	100	0.04	95	0.5	4	1.16
24% $Mo_{0.61}V_{0.31}Nb_{0.08}O_x/TiO_2$	533	100	0.05	92	0.01	6	1.12
$Mo_{0.61}V_{0.31}Nb_{0.08}O_x$	473	57	4	75	17	3	0.13
VO_x/TiO_2	483	100	14	67	0.1	19	0.81
MoO_x/TiO_2	473	17	94	1.5	0.7	3	0.003
MoO_x-VO_x/TiO_2	481	100	26	58	0.5	16	0.71

[a] Reaction conditions: partial pressure: ethanol: 32 kPa; O_2: 107 kPa; H_2O: 320 kPa, He: 1130 kPa and N_2: 11 kPa; total pressure: 1.6 MPa.

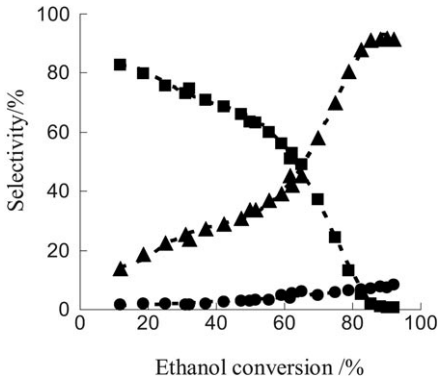

Figure 1. Ethanol oxidation at 473 K on $Mo_{0.61}V_{0.31}Nb_{0.08}O_x/TiO_2$. Total pressure: 1.6 MPa; partial pressures: Ethanol: 32 kPa; O_2: 107 kPa; H_2O: 320 kPa; He: 1130 kPa; N_2: 11 kPa. Product selectivities of (■) acetaldehyde, (▲) acetate (acetic acid and ethyl acetate) and (●) CO_x.

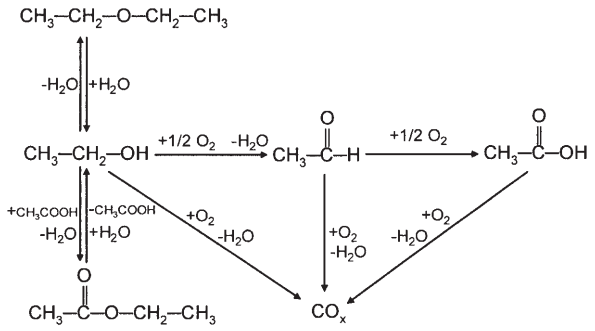

Scheme 1. Possible pathways of partial oxidation of ethanol.

acetate hydrolyzes to acetic acid as ethanol reactants are depleted. Traces of diethyl ether formed via ethanol dehydration on acidic sites. The selectivity towards acetate compounds (acetic acid and ethyl acetate) increased with ethanol conversion, because primary acetaldehyde products react to form acetic acid in sequential reactions (Scheme 1). CO_x selectivities increased with increasing conversion, as expected from the preferential formation of CO_x via secondary oxidation of acetaldehyde and acetic acid (Figure 1). The CO_x selectivities extrapolated to zero ethanol conversion were about 1% (Figure 1), indicating that only trace amounts of CO_x formed via direct combustion of ethanol reactants.

A proposed sequence of elementary steps for ethanol oxidation is shown in Scheme 2, in which O* represents a lattice oxygen ($M_i=O$, M_i-O-M_j, where M_i, $M_j=Mo^{6+}$, V^{5+}, or Nb^{5+}), CH_3CH_2O* is an ethoxide species attached to a M_i cation (C_2H_5-O-M_i), and CH_3CHO* and CH_3CHO_2* are adsorbed acetaldehyde and acetic acid species, respectively. *OH denotes a hydroxyl group and * represents a reduced metal center, consisting of an oxygen vacancy in the reducible mixed oxides. Typically, catalytic reactions involving lattice oxygen atoms and Mars van Krevelen redox cycles are limited by the elementary steps in the reduction part of the cycle, which includes the required C–H bond activation

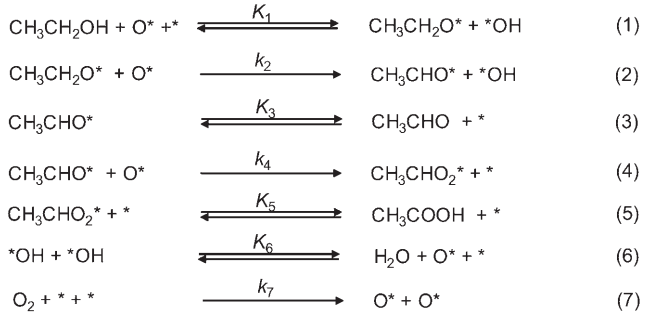

Scheme 2. Mars van Krevelen redox cycle for ethanol oxidation on Mo-V-Nb oxide catalysts.

steps.[15] In Scheme 2, step 1 involves quasi-equilibrated dissociative chemisorption of ethanol to form ethoxide species, from which lattice oxygen atoms abstract hydrogen in kinetically relevant steps to form chemisorbed acetaldehyde and *OH. These *OH groups recombine to form H_2O leaving behind an oxygen vacancy (step 6); lattice oxygen atoms are ultimately restored via irreversible dissociative chemisorption of O_2 co-reactants (step 7). Adsorbed acetaldehyde reacts with lattice oxygen atoms to form adsorbed acetate species (step 4), which then desorb as acetic acid (step 5).

Acetaldehyde is the predominant product at low ethanol conversions and, therefore, steps 4 and 5 become unimportant under such conditions. The elementary steps in Scheme 2 under the assumptions that: 1) all intermediates are at pseudosteady-state; 2) steps 1 and 6 are quasi-equilibrated, and 3) O*, *OH, * and C_2H_5O* are the most abundant reactive intermediates, lead to an equation for the rate of ethanol oxidation [Eq. (8)]:

$$rate=\frac{\alpha_1\left(\frac{P_{CH_3CH_2OH}{}^4}{P_{O_2}\cdot P_{H_2O}{}^2}\right)^{1/3}}{\left[1+\alpha_2\left(\frac{P_{CH_3CH_2OH}{}^2}{P_{O_2}{}^2\cdot P_{H_2O}}\right)^{1/3}+\alpha_3\left(\frac{P_{CH_3CH_2OH}\cdot P_{H_2O}}{P_{O_2}}\right)^{1/3}+\alpha_4\left(\frac{P_{CH_3CH_2OH}{}^4}{P_{O_2}\cdot P_{H_2O}{}^2}\right)^{1/3}\right]^2} \quad (8)$$

where α_1, α_2, α_3, α_4 are given by Equations (9)–(12), respectively.

$$\alpha_1=\frac{K_1{}^{4/3}\cdot k_2{}^{4/3}\cdot K_6{}^{2/3}}{k_7{}^{1/3}} \quad (9)$$

$$\alpha_2=\frac{k_2{}^{2/3}\cdot K_1{}^{2/3}\cdot K_6{}^{1/3}}{k_7{}^{2/3}} \quad (10)$$

$$\alpha_3=\frac{K_1{}^{1/3}\cdot k_2{}^{1/3}}{K_6{}^{1/3}\cdot k_7{}^{1/3}} \quad (11)$$

$$\alpha_4=\frac{K_1{}^{4/3}\cdot k_2{}^{1/3}\cdot K_6{}^{2/3}}{k_7{}^{1/3}} \quad (12)$$

At the high H_2O pressures in this study, *OH is likely to prevail as the most abundant adsorbed species, an assumption confirmed by the kinetic data reported below. As a

result the third term in the denominator becomes dominant and ethanol oxidation rates are given by Equations (13) and (14):

$$rate = \frac{k_{eff} \cdot {P_{O_2}}^{1/3} \cdot {P_{CH_3CH_2OH}}^{2/3}}{{P_{H_2O}}^{4/3}} \quad (13)$$

$$k_{eff} = {k_7}^{1/3} \cdot {k_2}^{2/3} \cdot {K_1}^{2/3} \cdot {K_6}^{4/3} \quad (14)$$

The effects of ethanol and O_2 pressure on reaction rates are shown in Figure 2 as a function of residence time. Rates extrapolated to zero residence time give reaction orders in ethanol (0.62) and O_2 (0.27) consistent with those predicted from Equation (13) when *OH is the most abundant adsorbed species (0.67 and 0.33, respectively).

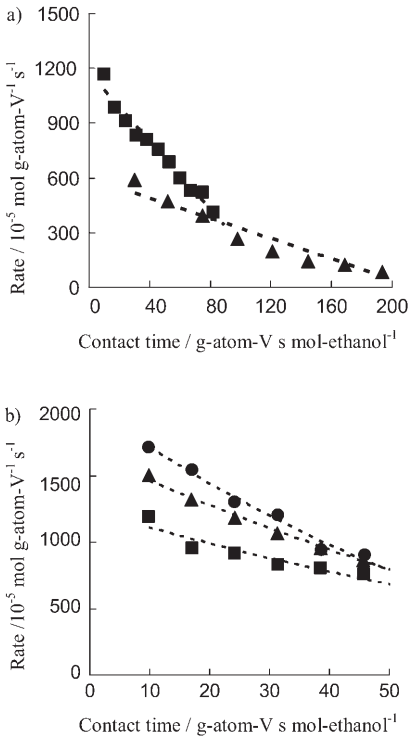

Figure 2. Catalytic performance of $Mo_{0.61}V_{0.31}Nb_{0.08}O_x/TiO_2$ for ethanol oxidation at 473 K. Total pressure: 1.6MPa; partial pressures: a) ethanol: (■) 32 kPa and (▲) 11 kPa; O_2: 107 kPa; N_2: 11 kPa; H_2O: 320 kPa; He: balance; b) ethanol: 32 kPa; O_2: (■) 107 kPa, (▲) 224 kPa and (●) 513 kPa; N_2: 11 kPa; H_2O: 320 kPa; He: balance.

The effects of H_2O partial pressure on ethanol oxidation rates at low conversions (<10%; acetaldehyde selectivity >83%) are shown in Figure 3. Reaction rates decreased as H_2O pressure increased, consistent with the functional form of the rate equation [Eq. (13)]. These data indicate that ethanol oxidation is inhibited by H_2O, although these inhibition effects are somewhat weaker than predicted from Equation (13).

The kinetic relevance of C–H bond activation steps in the chemisorbed ethoxide species (step 2), evident from the k_2 term in the effective rate constant [Eq. (14)], was probed by measuring the relative rates of C_2H_5OH and C_2D_5OD reactions with O_2 (Figure 4). Effective rate constants were 3.3 times larger for C_2H_5OH than for C_2D_5OD oxidation at 473 K. These kinetic isotope effects contain a kinetic contribution from step 2 (k_2), as well as smaller thermodynamic contributions from quasi-equilibrated steps 1 and 6 (K_1 and K_6). The relative contributions of each term are uncertain, but steps 1 and 2 would lead to normal kinetic isotope effects, as observed experimentally.

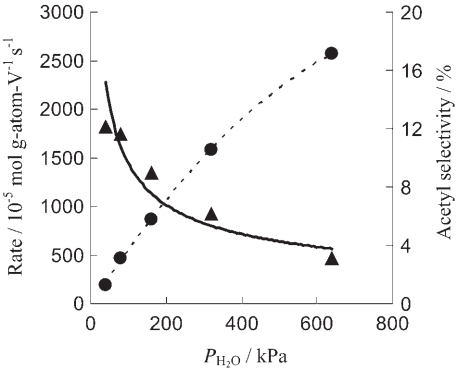

Figure 3. Ethanol conversion rate and acetate selectivity at 473 K on $Mo_{0.61}V_{0.31}Nb_{0.08}O_x/TiO_2$. Total pressure: 1.6 MPa; partial pressures: Ethanol: 32 kPa; O_2: 107 kPa; water: 0–640 kPa; N_2: 11 kPa; He: Balance. The solid line represents the dependence predicted from Equation (13).

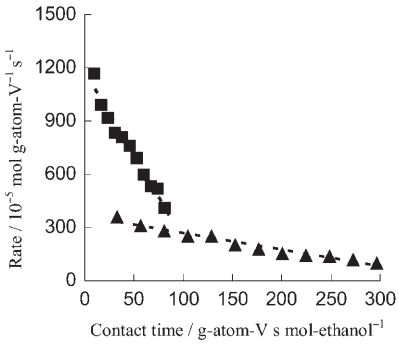

Figure 4. Ethanol ((■) C_2H_5OH or (▲) C_2D_5OD) oxidation reaction rate at 473 K on $Mo_{0.61}V_{0.31}Nb_{0.08}O_x/TiO_2$. Total pressure: 1.6 MPa; partial pressures: Ethanol: 32 kPa; O_2: 107 kPa; water: 320 kPa; He: 1130 kPa; N_2: 11 kPa.

The kinetic analysis described above was carried out by extrapolating rates to zero conversion by using reaction time data or rates at low ethanol conversion, for which acetic acid and its ester are present at low concentrations. At higher ethanol conversions, acetic acid is formed by sequential steps that oxidize acetaldehyde(step 4 in Scheme 2). The assumption of quasi-equilibrium for acetaldehyde adsorption–desorption (step 3 in Scheme 2) leads to an expression for acetate selectivities (combined acetic acid and ethyl acetate) based on these elementary steps:

$$\frac{rate_{acetate}}{rate} = \frac{k_4 \cdot {k_7}^{1/3} \cdot {P_{O_2}}^{1/3} \cdot {P_{H_2O}}^{2/3} \cdot P_{CH_3CHO}}{{k_2}^{4/3} \cdot {K_1}^{4/3} \cdot K_3 \cdot {K_6}^{2/3} {P_{CH_3CH_2OH}}^{4/3}} \quad (15)$$

This expression indicates that acetic acid synthesis selectivities should increase with H_2O partial pressure, consistent with the data shown in Figure 5. H_2O increased the ratio of

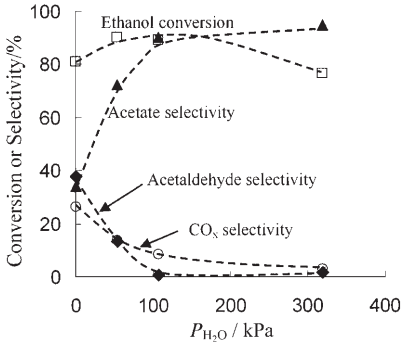

Figure 5. Catalytic performance of $Mo_{0.61}V_{0.31}Nb_{0.08}O_x/TiO_2$ for ethanol oxidation at 473 K at different water partial pressures. Total pressure: 1.6 MPa; partial pressures: Ethanol: 32 kPa; O_2: 107 kPa; N_2: 11 kPa; He: balance. Ethanol conversion (□) and selectivity of (◆) acetaldehyde, (▲) acetic acid and ethyl acetate and (○) CO_x.

acetic acid to acetaldehyde because it decreased the rate of acetaldehyde synthesis more effectively than the rate of oxidation of acetaldehyde to acetic acid, as shown by Equation (15). At high H_2O partial pressure (>107 kPa), acetaldehyde is almost undetectable and acetate is the only predominant product with selectivities of 90%. The higher stability of acetic acid relative to acetaldehyde, inferred from the energy of their respective weakest C–H bonds (acetic acid, $H{-}CH_2C(O)OH$ 398.7 kJ mol^{-1}; acetaldehyde, $CH_3C(O){-}H$, 374 kJ mol^{-1}[16]) leads, in turn, to the observed inhibition of CO_x selectivity by H_2O (from 26 to 3% with 320 kPa H_2O at 80% ethanol conversion). This reflects the scavenging of acetaldehyde by H_2O to form more stable acetic acid products, thus preventing the intervening oxidation of reactive acetaldehyde to CO_x.[17]

The role of individual MoO_x and VO_x species on oxidation rates was examined by comparing ethanol oxidation rates and selectivities on MoO_x or VO_x domains dispersed on TiO_2 at surface densities (vanadium: 9.0 molecules nm^{-2}, molybdenum: 4.8 molecules nm^{-2}) corresponding to near monolayer coverages (vanadium: 8.0 molecules nm^{-2},[18] molybdenum: 5.0 molecules nm^{-2}[19]). VO_x domains on TiO_2 showed high reactivity for ethanol oxidation, but MoO_x domains were much less reactive and formed predominantly acetaldehyde because of their lower reactivity and the lower concomitant ethanol conversions (Table 2). VO_x/TiO_2 catalysts gave 19 and 14% selectivities for CO_x and acetaldehyde, respectively, at 100% ethanol conversion; these selectivities are much higher than on $Mo_{0.61}V_{0.31}Nb_{0.08}O_x/TiO_2$ (4% CO_x and <1% acetaldehyde) under similar conditions. Ethanol oxidation on binary MoO_x-VO_x structures dispersed on TiO_2 (Table 2) gave similar rates and selectivities as VO_x/TiO_2, consistent with the active role of VO_x species in ethanol oxidation reactions. $Mo_{0.61}V_{0.31}Nb_{0.08}O_x/TiO_2$ catalysts are much more effective than VO_x/TiO_2 in the secondary conversion of acetaldehyde to more stable acetic acid products. Compared to VO_x/TiO_2, the slightly higher density of VO_x domains (14.5 V nm^{-2}) and the presence of MoO_x and NbO_x domains of $Mo_{0.61}V_{0.31}Nb_{0.08}O_x/TiO_2$ may have led to a marked decrease in the number of exposed V–O–Ti linkages, which appear to catalyze the unselective oxidation of acetaldehyde to CO_x.[20]

Conclusion

The catalytic conversion of ethanol to acetic acid in the gas phase was achieved with unprecedented rates and selectivities on Mo-V-Nb oxides precipitated in the presence of colloidal TiO_2. Acetic acid forms via sequential oxidation of primary acetaldehyde products, a step promoted by H_2O. The rapid scavenging of acetaldehyde to form more stable acetic acid prevents its intervening combustion to CO_2 and leads to acetic acid yields of >90% at 510 K. Kinetic and isotopic data are consistent with a reduction–oxidation catalytic cycle limited by C–H bond activation.

Experimental Section

$Mo_{0.61}V_{0.31}Nb_{0.08}O_x$ was prepared by a slurry method.[11a] A solution of $C_4O_8NbOH{\cdot}NH_3$ (2.42 g, Aldrich; 99.99%) was added slowly to a solution containing $C_2O_4H_2$ (7.2 g, Fluka, 99%), NH_4VO_3 (3.63 g, Sigma–Aldrich, 99%) and $(NH_4)_6Mo_7O_{24}{\cdot}4H_2O$ (10.77 g, Aldrich, 99.98%) while stirring at ambient temperature. Water was evaporated under dynamic vacuum at 363 K with stirring. The powders formed were treated at 393 K overnight and then in flowing dry air (Praxair, extra dry, 1.67 cm^3 s^{-1}) at 673 K, for 4 h. For the 24% $Mo_{0.61}V_{0.31}Nb_{0.08}O_x/TiO_2$ sample, TiO_2 (10 g, Degussa, P25, BET: 50 m^2 g^{-1}, anatase/rutile 3:1) was added to the solution before adding the $C_4O_8NbOH{\cdot}NH_3$ solution.

MoO_x/TiO_2 (5.3 wt% MoO_3) and VO_x/TiO_2 (6.1 wt% V_2O_5) were prepared by impregnating dehydrated TiO_2 (8 g, Degussa, P25) with (Aldrich, 99.8%) solutions of vanadyl isopropoxide (1.3 g, Aldrich, 98%) or molybdenyl acetylacetonate (1 g, Alfa Aesar, 99%) in toluene.[20] These samples were treated in flowing dry air at 673 K for 4 h after evaporating the toluene solvent. The MoO_x-VO_x/TiO_2 (2.65 wt% MoO_3 and 3.05 wt% V_2O_5) was prepared by impregnating the VO_x/TiO_2 (3.05 wt% V_2O_5) sample with a solution of molybdenyl acetylacetonate in toluene and was treated in flowing dry air at 673 K for 4 h after evaporating the toluene solvent.

CO_2 chemisorption data were collected by using a Quantachrome 1C Autosorb apparatus. Samples (~0.1 g of pellets) were heated in He at 0.083 K s^{-1} to 673 K and were held at 673 K for 2 h to remove adsorbed H_2O and CO_2 before CO_2 adsorption measurements. After cooling to 313 K, samples were evacuated and a CO_2 adsorption isotherm was obtained between 5.3 and 75 kPa CO_2 (Praxair, 99.998%). Chemisorption uptakes were calculated by extrapolation of the low-pressure linear part of the isotherm to zero pressure.

Ethanol (Aldrich, anhydrous, 99.5%) oxidation rates and selectivities were measured by using a stainless-steel tubular reactor at 1.6 MPa. The temperature of the catalyst bed was measured by a K-type thermocouple located within a concentric thermowell. Catalyst pellets (size: 0.25–0.50 mm) diluted by acid-washed quartz of similar size (Aldrich, White quartz, diluted to catalyst bed weight of 3 g) were treated in a mixture of

He (Praxair, 99.999%, 0.49 $cm^3 s^{-1}$) and N_2/O_2 (Praxair mixture, 10% N_2 in O_2, certified, 0.09 $cm^3 s^{-1}$) flows at 673 K for 2 h. Kinetic studies were performed at 473–533 K. High-pressure syringe pumps (Teledyne Isco Inc., model 500 D) were used to introduce H_2O (deionized) and ethanol. An on-line gas chromatograph (HP 5890, Series II), equipped with a flame ionization detector (FID) and a thermal conductivity detector (TCD) were used to measure the concentration of all species in the reactor effluent. N_2, O_2, CO, CO_2, and H_2O were analyzed by a HP Plot Q capillary column (30 m × 0.32 mm) connected to a TCD detector. Ethene, ethanol, acetaldehyde, ethyl acetate, and acetic acid were analyzed by a HP Plot U capillary column (30 m × 0.32 mm) connected to a flame ionization detector.

Deuterated ethanol (C_2D_5OD, 99% D, anhydrous, Cambridge isotopes) and ethanol reactions were also carried out in a stainless-steel gradientless batch recirculating reactor at 1.6 MPa. In order to avoid the condensation of water and acetic acid, all the wetted parts were maintained at a constant temperature of 433 K. The reactor contents (volume = 206 cm^3) were recirculated at 20 $cm^3 s^{-1}$ (STP) by using a graphite gear micropump (Micropump 182-336). The protocols for analysis of reactants and products were similar to those described above.

Appendix

Derivation of rate expressions: At low ethanol conversion, acetaldehyde is the predominant product. Thus, the steps that lead to formation of acetate species will not be taken into account in deriving initial ethanol oxidation rates. The rate of this reaction (see [Eq. (16)]) can be obtained from the rate of any irreversible steps in Scheme 2, for example, step 2:

$$rate = k_2 \cdot [CH_3CH_2O^*] \cdot [O^*] \tag{16}$$

The quasi-equilibrium assumption for steps 1 and 6 in Scheme 2 leads to expressions (17) and (18) for $[CH_3CH_2O^*]$ and [*OH],

$$[CH_3CH_2O^*] = \frac{K_1 \cdot P_{CH_3CH_2OH} \cdot [O^*] \cdot [^*]}{[^*OH]} \tag{17}$$

$$[^*OH] = \left(\frac{P_{H_2O} \cdot [O^*] \cdot [^*]}{K_6} \right)^{1/2} \tag{18}$$

The differential equation describing the time-dependent response of O* is given by Equation (19):

$$d[O^*]/dt = k_7 \cdot P_{O_2} \cdot [^*]^2 - k_2 \cdot [CH_3CH_2O^*] \cdot [O^*] \tag{19}$$

Application of pseudo-steady-state hypothesis for O* then gives Equation (20):

$$[^*] = \frac{{k_2}^{2/3} \cdot {K_1}^{2/3} \cdot {K_6}^{1/3} \cdot {P_{CH_3CH_2OH}}^{2/3} \cdot [O^*]}{{k_7}^{2/3} \cdot {P_{O_2}}^{2/3} \cdot {P_{H_2O}}^{1/3}} \tag{20}$$

And the concentrations of $[CH_3CH_2O^*]$ and [*OH] can then be expressed in terms of [O*] as (21) and (22),

$$[CH_3CH_2O^*] = \frac{{K_1}^{4/3} \cdot {k_2}^{1/3} \cdot {K_6}^{2/3} \cdot {P_{CH_3CH_2OH}}^{4/3} \cdot}{{k_7}^{1/3} \cdot {P_{O_2}}^{1/3} \cdot {P_{H_2O}}^{2/3}} \cdot [O^*] \tag{21}$$

$$[^*OH] = \frac{{K_1}^{1/3} \cdot {k_2}^{1/3} \cdot {P_{H_2O}}^{1/3} \cdot {P_{CH_3CH_2OH}}^{1/3}}{{K_6}^{1/3} \cdot {k_7}^{1/3} \cdot P_{O_2}{}^{1/3}} \cdot [O^*] \tag{22}$$

A site balance that includes O*, *, $CH_3CH_2O^*$, and *OH combined with the equations above then gives an expression (23) for [O*] as a function of the partial pressures of gas-phase species:

$$[O^*] = \left[1 + \frac{{k_2}^{2/3} \cdot {K_1}^{2/3} \cdot {K_6}^{1/3} \cdot {P_{CH_3CH_2OH}}^{2/3}}{{k_7}^{2/3} \cdot {P_{O_2}}^{2/3} \cdot {P_{H_2O}}^{1/3}} + \frac{{K_1}^{1/3} \cdot {k_2}^{1/3} \cdot {P_{H_2O}}^{1/3} \cdot {P_{CH_3CH_2OH}}^{1/3}}{{K_6}^{1/3} \cdot {k_7}^{1/3} \cdot {P_{O_2}}^{1/3}} + \frac{{K_1}^{4/3} \cdot {k_2}^{1/3} \cdot {K_6}^{2/3} \cdot {P_{CH_3CH_2OH}}^{4/3}}{{k_7}^{1/3} \cdot {P_{O_2}}^{1/3} \cdot {P_{H_2O}}^{2/3}} \right]^{-1} \tag{23}$$

The oxidation rate is then given by substituting this into the rate of step 2:

$$rate = ({k_2}^{4/3} \cdot {K_1}^{4/3} \cdot {K_6}^{2/3} \cdot {P_{CH_3CH_2OH}}^{4/3}) \cdot ({k_7}^{1/3} \cdot {P_{O_2}}^{1/3} \cdot {P_{H_2O}}^{2/3})^{-1} \cdot \left[1 + \frac{{k_2}^{2/3} \cdot {K_1}^{2/3} \cdot {K_6}^{1/3} \cdot {P_{CH_3CH_2OH}}^{2/3}}{{k_7}^{2/3} \cdot {P_{O_2}}^{2/3} \cdot {P_{H_2O}}^{1/3}} + \frac{{K_1}^{1/3} \cdot {k_2}^{1/3} \cdot {P_{H_2O}}^{1/3} \cdot {P_{CH_3CH_2OH}}^{1/3}}{{K_6}^{1/3} \cdot {k_7}^{1/3} \cdot {P_{O_2}}^{1/3}} + \frac{{K_1}^{4/3} \cdot {k_2}^{1/3} \cdot {K_6}^{2/3} \cdot {P_{CH_3CH_2OH}}^{4/3} \cdot}{{k_7}^{1/3} \cdot {P_{O_2}}^{1/3} \cdot {P_{H_2O}}^{2/3}} \right]^{-2} \tag{24}$$

At high ethanol conversion, acetic acid is formed from acetaldehyde. Application of quasi-equilibrium assumptions for step 3 leads to the expression (25) for $[CH_3CHO^*]$,

$$[CH_3CHO^*] = \frac{P_{CH_3CHO} \cdot [^*]}{K_3} \tag{25}$$

Therefore, the fraction of ethanol converted to acetic acid can be expressed by Equation (26):

$$\frac{rate_{acetate}}{rate} = \frac{k_4 \cdot \frac{P_{CH_3CHO} \cdot [^*]}{K_3} \cdot [O^*]}{k_2 \cdot K_1 \cdot P_{CH_3CH_2OH} \cdot [O^*]^2 \cdot \frac{[^*]}{[^*OH]}} = \frac{k_4 \cdot {k_7}^{1/3} \cdot {P_{O_2}}^{1/3} \cdot {P_{H_2O}}^{2/3} \cdot P_{CH_3CHO}}{{k_2}^{4/3} \cdot {K_1}^{4/3} \cdot K_3 \cdot {K_6}^{2/3} \cdot {P_{CH_3CH_2OH}}^{4/3}} \tag{26}$$

Acknowledgements

Financial support from Exxon Mobil Research and Engineering Co. is gratefully acknowledged. The authors acknowledge fruitful discussions with Dr. Beata Kilos.

[1] G. Cainelli, G. Cardillo, *Chromium Oxidations in Organic Chemistry*, Springer, Berlin, **1984**.
[2] A. Shaabani, D. G. Lee, *Tetrahedron Lett.* **2001**, *42*, 5833–5836.
[3] a) K. Sato, M. Aoki, R. Noyori, *Science* **1998**, *281*, 1646–1647; b) G.-J. ten Brink, I. W. C. E. Arends, R. A. Sheldon, *Science* **2000**, *287*, 1636–1639.
[4] T. Mallat, A. Baiker, *Catal. Today* **1994**, *19*, 247–284.
[5] K. Ebitani, Y. Fujie, K. Kaneda, *Langmuir* **1999**, *15*, 3557–3562.
[6] a) K. Yamaguchi, N. Mizuno, *Angew. Chem.* **2002**, *114*, 4720–4724; *Angew. Chem. Int. Ed.* **2002**, *41*, 4538–4542; b) K. Yamaguchi, K. Mori, T. Mizugaki, K. Ebitani, K. Kaneda, *J. Am. Chem. Soc.* **2000**, *122*, 7144–7145.
[7] Y. Obana, H. Uchida, K. Sano, WO 2000061535, **2000**.
[8] C. H. Christensen, B. Jøgensen, J. Rass-Hansen, K. Egeblad, R. Madsen, S. K. Klitgaard, S. M. Hansen, M. R. Hansen, H. C. Andersen, A. Riisager, *Angew. Chem.* **2006**, *118*, 4764–4767; *Angew. Chem. Int. Ed.* **2006**, *45*, 4648–4651.
[9] a) F. Gonçalves, P. R. S. Medeiros, J. G. Eon, L. G. Appel, *Appl. Catal. A* **2000**, *193*, 195–202; b) P. R. S. Medeiros, J. G. Eon, L. G. Appel, *Catal. Lett.* **2000**, *69*, 79–82.
[10] M. Gubelmann-Bonneau, S. A. Rhodia, US 5840971, **1998**.
[11] a) E. M. Thorsteinson, T. P. Wilson, F. G. Young, P. H. Kasai, *J. Catal.* **1978**, *52*, 116–132; b) P. Botella, E. García-González, A. Dejoz, J. M. López Nieto, M. I. Vázquez, J. González-Calbet, *J. Catal.* **2004**, *225*, 428–438; c) F. Ivars, P. Botella, A. Dejoz, J. M. López Nieto, P. Concepción, M. I. Vázquez, *Top. Catal.* **2006**, *38*, 59–

67; d) H. Borchert, U. Dingerdissen, J. Weiguny, German Patent DE 19620542, **2000**; e) H. Borchert, U. Dingerdissen, German Patent DE 19630832, **2001**.
[12] J. H. McCain, S. W. Kaiser, EP 294846, **1988**.
[13] X. Li, E. Iglesia, unpublished results.
[14] a) S. Rondon, M. Houalla, D. M. Hercules, *Surf. Interface Anal.* **1998**, *26*, 329–334; b) D. G. Barton, M. Shtein, R. D. Wilson, S. L. Soled, E. Iglesia, *J. Phys. Chem. B* **1999**, *103*, 630–640.
[15] a) A. Khodakov, J. Yang, S. Su, E. Iglesia, A. T. Bell, *J. Catal.* **1998**, *177*, 343–351; b) K. Chen, S. Xie, A. T. Bell, E. Iglesia, *J. Catal.* **2001**, *198*, 232–242.
[16] Y. R. Luo, J. A. Kerr, *Handbook of Chemistry and Physics*, CRC, Boca Raton, **2006**, pp. 9–61.
[17] a) C. Batiot, B. K. Hodnett, *Appl. Catal. A* **1996**, *137*, 179–191; b) F. E. Cassidy, B. K. Hodnett, *CATTECH* **1998**, *2*, 173–180.
[18] G. Centi, *Appl. Catal. A* **1996**, *147*, 267–298;.
[19] a) F. Prinetto, G. Cerrato, G. Ghiotti, A. Chiorino, M. C. Campa, D. Gazzoli, V. Indovina, *J. Phys. Chem.* **1995**, *99*, 5556–5567; b) Y. Chen, L. F. Zheng, *Catal. Lett.* **1992**, *12*, 51–62.
[20] S. Yang, E. Iglesia, A. T. Bell, *J. Phys. Chem. B* **2005**, *109*, 8987–9000.

Received: April 13, 2007
Revised: July 27, 2007
Published online: October 2, 2007

